University Library

MINERVA ACCESS

A gateway to Melbourne's research publications

Minerva Access is the Institutional Repository of The University of Melbourne

Author/s:
Peng, M;Tian, Y;Gaudin, C

Title:
Investigations into the Uplift of Skirted Foundations on Clay at Varying Rates

Date:
2024-02-01

Citation:
Peng, M., Tian, Y. & Gaudin, C. (2024). Investigations into the Uplift of Skirted Foundations on Clay at Varying Rates. Journal of Geotechnical and Geoenvironmental Engineering, 150 (2), pp.04023137-. https://doi.org/10.1061/JGGEFK.GTENG-11502.

Persistent Link:
https://hdl.handle.net/11343/340373

Investigations into the uplift of skirted foundations on clay at varying rates

Maozhu Peng
PhD student
Centre for Offshore Foundation Systems and Ocean Graduate School
The University of Western Australia
35 Stirling Highway, Crawley WA 6009, Australia
Email: maozhu.peng@research.uwa.edu.au

Yinghui Tian (corresponding author)
ARC Future Fellow
Department of Infrastructure Engineering
The University of Melbourne
Parkville, Victoria 3010, Australia
Email: yinghui.tian@unimelb.edu.au

Christophe Gaudin
Professor
Centre for Offshore Foundation Systems and Ocean Graduate School
The University of Western Australia
35 Stirling Highway, Crawley WA 6009, Australia
Email: christophe.gaudin@uwa.edu.au

Submitted as Technical Paper
Words: ~3563 (excluding references and acknowledgment)
Figures: 11
Tables: 1

Investigations into the uplift skirted foundations on clay at varying rates

Abstract

This paper presents finite element simulations to re-interpret a series of full model and PIV centrifuge tests to study the uplift of skirted foundations. The focus is on the influence of uplift rate on the uplift capacity and the mechanism of "breakaway" (i.e., the phenomenon of sudden loss of uplift resistance). A backbone curve, quantifying the uplift rate-capacity relationship, is established for uplift based on the numerical and experimental results. The dimensionless velocities V = 6 and 130 are found to be the boundaries for drained, partially drained, and undrained conditions. The breakaway is found related to ambient water infiltration. In the numerical modelling, the remaining length of the skirt inside soil is used as an indicator for breakaway, i.e., breakaway happens when this length is smaller than a critical value. This hypothesis is demonstrated to be effective by comparing the numerical modelling with the experimental results.

Keywords: skirted foundation uplift; hydro-mechanical interface; breakaway; viscosity; rate effect; drainage

Notation list

s_u, s_{um}, s_{u0}	Soil undrained strength, soil strength at mudline, and soil strength at skirt tip
s_{um}	Soil undrained strength at mudline
s_{u0}	Soil undrained strength at skirt tip
k	Soil undrained strength gradient against depth
z	Depth below mudline
D	Foundation diameter
d	Skirt length
$N_c, N_{c,\mathrm{drainge}}$	Uplift capacity factor of foundation and its value without strain rate effect
A	Cross-section area of foundation
v	Uplift velocity
V, V_{ref}	Dimensionless uplift velocity and reference dimensionless uplift velocity
c_v	Coefficient of consolidation
u, u_g, u_s	Suction, suction within interface, and suction within soil
K_0	Coefficient of lateral earth pressure at rest
φ	Soil internal friction angle
p_p	Surcharge at mudline
γ'	Submerged unit weight of soil
γ_w	Water unit weight
v_t	Transverse flow rate of interface
c_t	Transverse conductivity of interface
g_n	Interface opening distance
K_r, K_{r0}	Longitudinal conductivity of interface and its value immediately before breakaway
K_{r0}	Longitudinal conductivity of interface before breakaway
r	Radial coordinate
q_r	Radial flux of interface
t	Time
d_r	Remaining length of skirt inside soil
ζ	Dimensionless breakaway factor
w, w_b	Uplift distance and uplift distance before breakaway

1 Introduction

Skirted foundations consist of a top plate and a circumferential skirt, confining a soil plug inside the compartment once fully installed. The uplift capacity and failure mechanism of skirted foundations vary depending on the drainage condition of the soil (Randolph & Gourvenec 2017; Bye et al. 1995; Watson & Humpheson 2007; Miller et al. 1996; Dendani & Colliat 2002; Gaudin et al. 2011), because the negative excess pore pressure (i.e. suction) below the top plate significantly affects the uplift process (Chen et al. 2012; Chatterjee et al. 2014; Acosta-Martinez et al. 2008).

From the available studies on skirted foundation uplift (e.g., Acosta-Martinez et al. 2008, 2010, 2012; Mana et al. 2013; Gourvenec et al. 2007; Chen et al. 2012), two critical issues can be found, requiring more fundamental investigations. One is the effect of loading rate on the uplift resistance, which strongly influences the pore water pressure generation and dissipation below the top plate. Compared with compression, the “backbone” curve (i.e., the relation between the peak uplift resistance and uplift velocity) for uplift has not been well established to distinguish the range between undrained, partially drained, and fully drained conditions. The other issue is “breakaway”, which is the phenomenon where the soil detached from the foundation, resulting in a rapid reduction of the uplift resistance down to nearly to zero. This is distinctly different from compression and requires further exploration.

This paper re-interprets a series of full model and PIV (half model) centrifuge tests of skirted foundation uplift at varying rates performed by Li (2015) with the aid of finite element (FE) simulations, focusing on investigating the rate effect and breakaway mechanism. A backbone curve in terms of the peak uplift resistance versus the dimensionless velocity is established from this study, where the dimensionless velocity ranges for drained, partially drained, and undrained conditions are quantified. From the observation of centrifuge tests and numerical

modelling, a criterion for predicting breakaway onset is proposed. A good agreement between the numerical prediction and physical observation are reached, and the mechanism of breakaway is discussed from the modelling results.

2 Centrifuge modelling

Li (2015) conducted a total of 23 centrifuge tests on the drum centrifuge (Stewart et al. 1998) at 200g at the University of Western Australia, including 18 full model tests and 5 half model PIV tests. The tests are re-interpreted in this paper thanks to the addition of new numerical modelling. The test procedures and results are reviewed briefly for completeness.

2.1 Soil sample

Commercially available kaolin power was mixed with water to a moisture content of 120% (twice the liquid limit) under vacuum and then consolidated in-flight at 200g, giving the soil sample an initial height of 150 mm. Then, the top 30 mm layer was scraped off, giving a final sample height 120 mm. T-bar tests were conducted before, during and after the tests, showing an approximately linear soil strength profile:

$$s_u = s_{um} + kz \tag{1}$$

where s_{um} is the soil strength at mudline, being 2.55kPa and 0.92 kPa for the full model and PIV tests, respectively, z the vertical distance to mudline and k the gradient for soil strength to increase with depth, being 1.21 kPa/m and 1.33 kPa/m for the full model and PIV tests (in prototype), respectively.

2.2 Test setup and instrumentation

As shown in Fig. 1, circular aluminium foundation models with a diameter D of 60 mm (12 m in prototype) were used. It had a skirt length d = 12 mm (2.4 m in prototype), giving an

embedment ratio d/D = 0.2 (noting the top plate was contacting the soil surface before the uplift tests). The layout in centrifuge is shown in Fig. 1(b).

2.3 Test procedures

For the full model tests, the foundation was installed with a speed of 0.05 mm/s at 1g. After installation, the centrifuge ramped up to 200g. Then, the centrifuge channel was filled with 30 mm water to submerge the model. A preload of 15.4 N was applied onto the foundation for approximately 10 mins in model scale in order for the top plate to have better contact with the soil. This preload is 10% of the foundation undrained bearing capacity, estimated as $0.1N_c s_{u0}A$, where the dimensionless bearing capacity factor was taken as N_c = 10 following Mana et al. (2010), s_{u0} = 5.45 kPa the soil strength at skirt tip, and A the cross-section area of the foundation. After the preloading, the foundation was uplifted by the actuator at a constant velocity. Nine tests were conducted where the foundation uplift velocities are v = 0.0005, 0.001, 0.005, 0.01, 0.05, 0.1, 0.5, 1, 3 mm/s (in model scale), respectively. The velocity can be expressed as dimensionless velocities $V = vD/c_v$ (Finnie & Randolph, 1994). Taking the consolidation coefficient c_v of kaolin clay at the experimental stress level as 1.5 m^2/year (House et al., 2001), the 9 tests have V= 0.6, 1.3, 6.3, 12.6, 63.1, 126.1, 630.7, 1261.4, 3784.3, respectively.

For the PIV tests, a half model was used and kept tight contact to the transparent window of the strongbox during the tests. The foundation and soil movements were recorded by a camera in front of the transparent window in flight. The test procedures were the same as in full model tests and 3 PIV tests were conducted at rate of v = 0.001; 0.05 and 1 mm/s (i.e., V=1.3, 63.1, and 1261.4).

2.4 Test results

The resistance and excess pore pressure of the 9 full model centrifuge tests (V=0.6, 1.3, 6.3, 12.6, 63.1, 126.1, 630.7, 1261.4, 3784.3) are shown in Fig. 2. The upper part is the

dimensionless uplift resistance F/As_{u0}, where F is the uplift resistance force, A the cross-sectional area of the foundation, and s_{u0} the undrained soil strength at the skirt tip. The lower part is the dimensionless excess pore pressure u/s_{u0}. The horizontal axis is the uplift distance w normalised by the skirt length d. At $V \leq 1.3$, the uplift resistance F/As_{u0} is close to zero throughout, and there is no obvious breakaway occurring. At higher velocities, the resistance first increases to a peak, followed by some mild softening before an abrupt breakaway happening. It can be noted that the peak resistance increases with uplift velocity.

At peak uplift resistance, the soil flow mechanism derived from the 3 PIV tests (V = 1.3, 63.1, 1261.4, representing slow, intermediate, and fast uplift) is shown in Fig. 3, where the left half is the displacement contour plot (normalised by the foundation displacement) and the right half is the soil movement vector plot. The failure mechanisms at the three velocities are deemed to be in undrained, partially drained, and drained conditions (cross refer to the uplift resistance in Fig. 2).

The centrifuge results in Fig. 2 show that the development of the suction (negative excess pore pressure) below the foundation almost mirrors the uplift resistance for all the tests. This implies that nearly all the resistance to uplift is from negative pore pressure. When breakaway initiates, there is a sudden loss of suction, indicating that breakaway is related to a sudden change of hydraulic conditions around the foundation.

3 Numerical modelling

3.1 Model

As shown in Fig. 4, a 2D axisymmetric model was established with a soil domain size $5D \times 2D$. This size had been verified sufficient to eliminate boundary effects from preparatory sensitivity study. The soil bottom was fixed in all directions, while the two sides were allowed

to move only in vertical direction. The top surface was set as a free drainage boundary except the area covered by the foundation.

The foundation was modelled as a rigid body. A coupled hydro-mechanical interface was developed by the authors (see Peng et al., 2022 for details) and further extended to axisymmetric condition, which allows suction generation and dissipation and foundation-soil separation to be adequately addressed. The skirt-soil interaction was modelled as Coulomb friction contact model with the coefficient of friction α taken as 0.1 based on back analysis. It is noted that the model foundation was manufactured from aluminium with very smooth surfaces.

3.2 Soil constitutive model

Modified Cam Clay (MCC) (Roscoe & Burland, 1968; Schofield & Wroth, 1968) constitutive model was used to describe the soil behaviours. MCC parameters for the kaolin clay used in the centrifuge tests are listed in Table.1 (Steward, 1982). The soil was considered as K_0 consolidated with K_0 estimated as (Jaky 1944):

$$K_0 = 1 - \sin\varphi \approx 0.6 \tag{2}$$

It is crucial to keep the undrained shear strength s_u profile same as the experimental condition for a realistic modelling. In the numerical model, a surcharge p_p was applied on the mudline to improve numerical stability. The soil unit weight γ' and surcharge p_p were adjusted to provide a good fit of the s_u profile, where p_p and γ' were selected as 8.91 kPa and 4.23 kN/m^3. The numerical value of γ' is slightly lower than the typical kaolin clay effective unit weight in the range of 5 ~ 8 kN/m^3, but this represents a best fit to the shear strength to reproduce real soil behaviour.

3.3 Interface modelling

A coupled hydro-mechanical zero-thickness interface was developed by the authors in plane strain condition (see Peng et al. 2022 for details), which has been proved to be able to model uplifting problems adequately. It is extended to axisymmetric condition as shown in the following. As illustrated in Fig. 5, the transverse and longitudinal flows are defined as:

$$v_t = c_t \left(u_g - u_s \right) \tag{3}$$

$$q_r = g_n \frac{K_r}{\gamma_w} \frac{\partial u_g}{\partial r} \tag{4}$$

where v_t is the transverse flow rate; u_g the excess pore pressure at mid-gap, u_s the excess pore pressure of soil under the foundation; q_r the longitudinal flux, g_n the dimension of gap opening between the foundation and soil; K_r the longitudinal conductivity of the interface, γ_w the unit weight of water; and r denotes longitudinal distance. c_t is a parameter controlling the speed of fluid exchange between gap and soil plug, taken as 1.86×10^{-8} m/(kPa·s) based on back analysis of the centrifuge results.

According to continuity, the volumetric change of the interface (i.e., the space of between the foundation and the soil plug) equals the water flow-in volume minus the water flow-out volume. Assuming the water as incompressible:

$$-\frac{1}{r}\frac{dq_r}{dr} + v_t + \frac{\partial g_n}{\partial t} = 0 \tag{5}$$

where t denotes time.

3.4 Breakaway modelling

Based on the centrifuge observations, breakaway is assumed to initiate when the skirt length left in the soil d_r reaches a critical value ζd, where ζ is a value to be derived from the tests.

This is illustrated in Fig. 5, where the interface longitudinal conductivity K_r is assumed to vary with d_r. d_r initially equals to d and reduces with the uplift process. When $d_r > \zeta d$, K_r is set to increase linearly from 0 to K_{r0}. When d_r reaches ζd, K_r quickly increases to a large number by employing an expression $K_r = K_{r0}/(d_r/\zeta d)^b$, where b is taken as 100 in this study to ensure a rapid increase. The values of K_{r0} and ζ were taken as 3.2×10^{-9} m/s and 0.26, respectively, by back-analyzing numerical result to centrifuge data at V = 63.1. Note the same values are used for the analyses at other velocities.

3.5 Numerical result verification

Fig. 6 shows the comparisons between numerical and experimental results at V = 0.6, 63.1, and 3784.3. It can be seen that the numerical results agree well with the centrifuge tests, especially for V = 0.6 and 63.1. At V = 3784.3, the numerical result lies within the limit analysis solutions from Martin (2001), i.e., upper and lower bounds for undrained capacity of skirted foundations of 10.36 and 9.11. Also shown is the numerical result of Mana et al. (2010) with a good agreement with this study. The centrifuge result is higher than numerical result at V = 3784.3, which is believed due to soil undrained strength increases with strain rate (see Einav & Randolph, 2005), while the adopted MCC model does not consider this effect. The comparison of numerical and experimental results at other velocities can be found in Fig. 8.

It is clear that breakaway is well reproduced at all velocities. Note the values of ζ and K_{r0} are the same for all cases, and they were calibrated from the single case of V = 63.1 experimental result. The good agreement for all velocities indicates the breakaway modelling is effective.

4 The role of negative pore pressure (suction) in uplifting problem

From Fig. 2, it can be seen that the suction is the main component of the uplift resistance, and thus the skirt friction accounts for only a limited fraction, especially at fast velocities. At each

velocity, the recording of the three PPTs were comparable, within 3% difference, indicating an even distribution of pore pressure below the foundation.

It has been widely accepted that undrained uplift capacity equals the undrained compression capacity, i.e., the "reverse end bearing" mechanism (Acosta-Martinez et al. 2008; Mana et al., 2013). However, the effective soil stresses and pore pressure play different roles in undrained compression and uplift. For compression, both excess pore pressure and effective soil stresses provide resistance (see Tian et al., 2022 for more detailed discussion). With lower compression rate, the dissipation of excess pore pressure leads to consolidation (increase in soil effective stresses) and soil hardening, thus resulting in higher resistance with lower V (Finnie & Randolph, 1994; Randolph & Hope, 2004; Lehane et al., 2009; Chuang et al., 2006; Chow et al., 2020). In contrast, in uplift, suction is seen as the main component of resistance. With lower uplift rate, the suction dissipates, and thus uplift resistance drops correspondingly. Consequently, the drained uplift capacity is very low.

The stress paths for a soil point lying 0.03D below the foundation centre is shown in Fig. 7, where the sign of deviatoric stress q is defined as the same as the sign of $\sigma_v' - \sigma_h'$. At $V = 0.6$, the stress state merely changes during the uplift. At $V = 1.3 \sim 63.1$, the stress state mainly shows unloading into the yield surface. At higher velocities, the soil is first unloaded. After q reducing to zero, the soil is re-loaded again in extension ($\sigma_v' < \sigma_h'$) to reach the yield surface and moves towards the critical state line (CSL) following a stress path similar to undrained triaxial extension. But before reaching the CSL, another steep unloading occurs. This unloading is due to breakaway where the suction acting on the soil plug is quickly lost.

5 The rate effect and the backbone curves

Fig. 8 shows the dimensionless capacity factor $N_c = F_{\max}/Ds_{u0}$ versus the dimensionless velocity $V = vD/c_v$ for both the 9 centrifuge tests and the corresponding numerical modelling, where $F_{\max}$

is peak resistance. It can be seen that good agreement between experimental and numerical results is reached when $V < 80$. At greater velocities, the experimental results exceed the numerical results. This is believed due to the strain rate effect on the soil strength s_u, which the numerical modelling did not consider by using the MCC model.

The numerical results can be fitted by using the equation proposed by House et al. (2001):

$$\frac{N_{c,\text{drainage}}}{N_{c,\text{undrained}}} = a + \frac{b}{1 + cV^d} \tag{6}$$

where the subscript "drainage" represents the sole effect of drainage (without strain rate effect); a represents the contribution from skirt friction; $a + b = 1$ represents the undrained resistance factor at large V; and c and d control the sharpness of the curve. The best-fit values for a, b, c, and d are 0.01, 0.99, 183.36 and -1.52.

At $V < 6$, the uplift resistance stabilises to a small value, indicating drained conditions are reached. At $V > 130$, the uplift resistance stabilises at a peak, indicating undrained conditions are reached. This value is slightly higher than the undrained threshold $V = 30$ proposed by Finnie & Randolph (1994) based on a T-bar, and is much lower than the $V = 10000$ proposed by Chen et al. (2012) based on a surface footing. These differences are likely related to different easiness for ambient water infiltration, which decreases from surface footing to fully buried T-bar. The easier the infiltration, the faster the suction dissipation, and the higher the undrained threshold.

By combining the effect of strain rate, the below equation can be fitted to the experimental data, which can be regarded as a representative of soil viscous effect.

$$\frac{N_c}{N_{c,\text{drainage}}} = \left(\frac{V}{V_{\text{ref}}}\right)^m \tag{7}$$

where N_c is the dimensionless uplift capacity with both drainage and strain rate effects. V_{ref} and m are two constants, with the least-square best-fit values being 20 and 0.1, respectively.

Lehane et al. (2009) characterised a series of centrifuge tests studying the rate effect on T-bar behavior using the same equation as Eq. (7), with the value of m being 0.08, reasonably close to that in this study. It may seem surprising at first look that $N_c < N_{c,\text{driange}}$ when $V < V_{\text{ref}}$. This is actually because the numerical capacity at low V is slightly larger than the experimental one. But the difference is very small and thus ignored in this paper.

6 Discussion on breakaway

Fig. 2 shows that breakaway accompanies a sudden loss of suction below the foundation while some mild suction dissipation can be observed before breakaway. Fig. 9 shows the top plate and the underneath soil prior and post to the breakaway in PIV tests at v = 1 mm/s After breakaway, the space between the foundation and the soil obviously widened, indicating ambient water rapidly infiltrates into the foundation underside. The is possibly because the remaining length of the skirt inside soil d_r is too short to resist the ambient water infiltration. Therefore, this study assumed when d_r/d is less than a critical value ζ, breakaway initiates.

Fig. 10 compares the dimensionless uplift distance w_b/d when breakaway occurs for numerical and experimental observations, where w_b is the foundation uplift distance at breakaway, and d the skirt length. In general, good agreements are reached, indicating the breakaway is reasonably captured by the proposed method.

Fig. 11 shows the dimensionless gap opening g_n/d versus the displacement of the foundation w/d. For low velocities ($V \leq 12.6$), the gap opening equals the uplifting distance at any instant, showing that the behaviour is drained and water flows freely into the gap. For intermediate velocities (e.g., $V = 126.1$), the g_n/d increases nearly linearly with uplift distance, although the gap opening rate is slower than the uplift rate. At a certain point, the g_n/d increases sharply,

corresponding to the breakaway. The sudden widening of the gap during breakaway is in line with the PIV observation in Fig. 10. After breakaway, the slope of the curve becomes nearly equal to unity, indicating the uplift rate and gap opening rate are equal. For high velocities, the gap opening is small until breakaway occurs, showing the soil is essentially in undrained conditions before breakaway.

7 Concluding remarks

A series of centrifuge tests, including full model tests and half model PIV tests, were re-interpreted based on FE simulations to study the rate effect and breakaway during skirted foundation uplift.

Results indicate that, as uplift rate increases, the uplift resistance increases. A backbone curve for uplifting has been established, where $V = 6$ and $V = 130$ are seen to be the boundaries for drained, partially drained, and undrained conditions. The two components of the rate effect, drainage effect and strain rate effect, are quantified separately.

Breakaway is found associated with the rapid infiltration of ambient water into the foundation underside. In this study, breakaway is assumed to occur when the remaining length of the skirt inside soil becomes shorter than a critical value. This hypothesis is validated by the good agreement between numerical and experimental results.

A practical implication is that, for offshore foundations decommissioning and salvage of sunken vessels, uplift rate needs to be chosen carefully such that the uplift resistance can be minimized and the lifting period is reasonable. Besides, the current design of offshore foundations is conservative by neglecting the existence of suction, though more comprehensive and thorough studies are required to be conducted to improve our understanding

AKNOWLEDGEMENT

This research was undertaken with support from the Australia Research Council Discovery Projects DP190103315, DP180103314 and the second author's ARC Future Fellowship FT200100457. Former PhD student Xiaojun Li is acknowledged for his support and discussion of the centrifuge tests he carried out during his study.

References

Stewart DP, Boyle RS, Randolph MF. Experience with a new drum centrifuge. InCentrifuge 98 1998 (pp. 35-40).

Roscoe K, Burland JB. On the generalized stress-strain behaviour of wet clay.

Schofield A, Wroth P. Critical state soil mechanics. London: McGraw-Hill; 1968.

Wroth CP. The interpretation of in situ soil tests. Geotechnique. 1984 Dec;34(4):449-89.

Martin CM. Vertical bearing capacity of skirted circular foundations on Tresca soil. InInternational Conference on soil mechanics and geotechnical engineering 2001 (pp. 743-746).

Randolph M, Gourvenec S. Offshore geotechnical engineering. CRC press; 2017 Jul 12.

Chen R, Gaudin C, Cassidy MJ. Investigation of the vertical uplift capacity of deep water mudmats in clay. Canadian Geotechnical Journal. 2012 Jul;49(7):853-65.

Bye A, Erbrich C, Rognlien B, Tjelta TI. Geotechnical design of bucket foundations. InOffshore Technology Conference 1995 May 1. OnePetro.Watson PG, Randolph MF, Bransby MF. Combined lateral and vertical loading of caisson foundations. InOffshore technology conference 2000 May 1. OnePetro.

Miller DM, Brevig P. The Heidrun Field-Marine Operations. InOffshore Technology Conference 1996 May 6. OnePetro.

Dendani H, Colliat JL. Girassol: Design analysis and installation of the suction anchors. InOffshore Technology Conference 2002 May 6. OnePetro.

Gaudin C, Mohr H, Cassidy MJ, Bienen B, Purwana OA. Centrifuge experiments of a hybrid foundation under combined loading. InThe Twenty-first International Offshore and Polar Engineering Conference 2011 Jun 19. OnePetro.

Chatterjee S, Mana DS, Gourvenec S, Randolph MF. Large-deformation numerical modeling of short-term compression and uplift capacity of offshore shallow foundations. Journal of Geotechnical and Geoenvironmental Engineering. 2014 Mar 1;140(3):04013021.

House AR, Oliveira JR, Randolph MF. Evaluating the coefficient of consolidation using penetration tests. International Journal of Physical Modelling in Geotechnics. 2001 Sep;1(3):17-26.

Watson PG, Humpheson C. Foundation design and installation of the Yolla A platform. InOffshore Site Investigation and Geotechnics: Confronting New Challenges and Sharing Knowledge 2007 Sep 11. OnePetro.

Acosta-Martinez HE, Gourvenec SM, Randolph MF. An experimental investigation of a shallow skirted foundation under compression and tension. Soils and Foundations. 2008;48(2):247-54.

Acosta-Martinez HE, Gourvenec SM, Randolph MF. Effect of gapping on the transient and sustained uplift capacity of a shallow skirted foundation in clay. Soils and foundations. 2010;50(5):725-35.

Mana DS, Gourvenec S, Randolph MF. Experimental investigation of reverse end bearing of offshore shallow foundations. Canadian Geotechnical Journal. 2013;50(10):1022-33.

Gourvenec S, Martinez HA, Randolph M. Centrifuge model testing of skirted foundations for offshore oil and gas facilities. InOffshore Site Investigation and Geotechnics: Confronting New Challenges and Sharing Knowledge 2007 Sep 11. OnePetro.

Li, X. The uplift of offshore shallow foundations (Doctoral dissertation), University of Western Australia, 2015.

Mana DS, Gourvenec S, Randolph MF. A numerical study of the vertical bearing capacity of skirted foundations. InProc. 2nd Int. Symp. Front. Off. Geotech.(ISFOG), Perth 2010 Oct 4 (pp. 433-438).

Finnie IM, Randolph M. Punch-through and liquefaction induced failure of shallow foundations on calcareous sediments. InPunch-through and liquefaction induced failure of shallow foundations on calcareous sediments 1994 (pp. 217-230). Pergamon.

Jaky, J. (1944). The coefficient of earth pressure at rest. J. Soc. Hungarian Arch. Eng., 78(22), 355–358.

Einav I, Randolph MF. Combining upper bound and strain path methods for evaluating penetration resistance. International journal for numerical methods in engineering. 2005 Aug 14;63(14):1991-2016.

Tian Y, Ren J, Zhou T, Peng M, Cassidy MJ. Coupled hydro-mechanical interfaces to enable uplift modelling in offshore engineering. Ocean Engineering. 2022 Feb 1;245:110570.

Randolph M, Hope S. Effect of cone velocity on cone resistance and excess pore pressures. InEffect of cone velocity on cone resistance and excess pore pressures 2004 (pp. 147-152). Yodogawa Kogisha Co. Ltd.

Lehane BM, O'loughlin CD, Gaudin C, Randolph MF. Rate effects on penetrometer resistance in kaolin. Géotechnique. 2009 Feb;59(1):41-52.

Chung SF, Randolph MF, Schneider JA. Effect of penetration rate on penetrometer resistance in clay. Journal of geotechnical and geoenvironmental engineering. 2006 Sep;132(9):1188-96.

Chow SH, O'Loughlin CD, Zhou Z, White DJ, Randolph MF. Penetrometer testing in a calcareous silt to explore changes in soil strength. Géotechnique. 2020 Dec;70(12):1160-73.

Peng M, Tian Y, Gaudin C, Zhang L, Sheng D. Application of a coupled hydro-mechanical interface model in simulating uplifting problems. International Journal for Numerical and Analytical Methods in Geomechanics. 2022. https://doi.org/10.1002/nag.3450

Table 1. Parameters for MCC constitutive model

Parameter input for finite-element analysis	Values
Unit weight of water, γ_w: kN/m^3	10
Slope of swelling and recompression line in e-ln(p') space, κ	0.044
Slope of virgin compression line in e-ln(p') space, λ	0.205
Friction angle in triaxial compression, φ	23.5^o
Void ratio at p' = 1 kPa on critical state line, e_{cs}	2.14
Soil permeability, k_s: m/s	10^{-9}

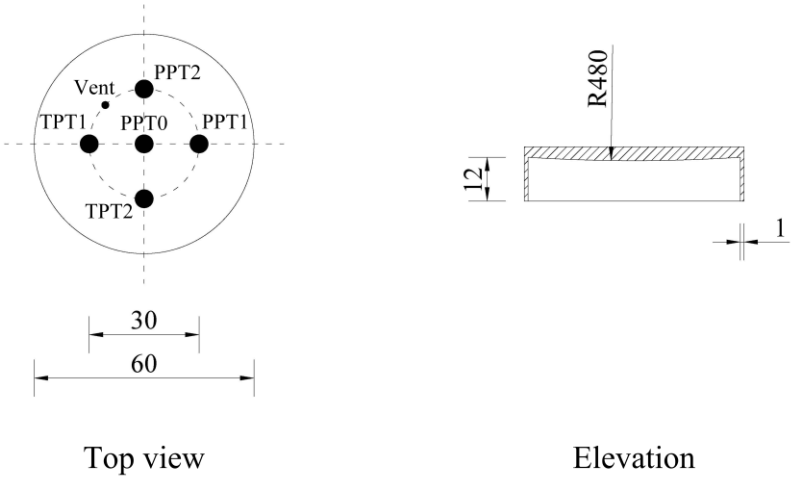

(a) Sketch of foundations

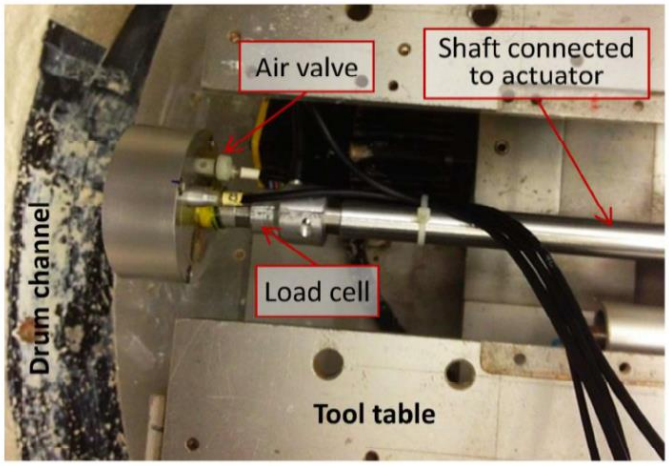

(b) Foundation layout in centrifuge

Fig. 1 Layout of the skirted foundations used in full model centrifuge tests

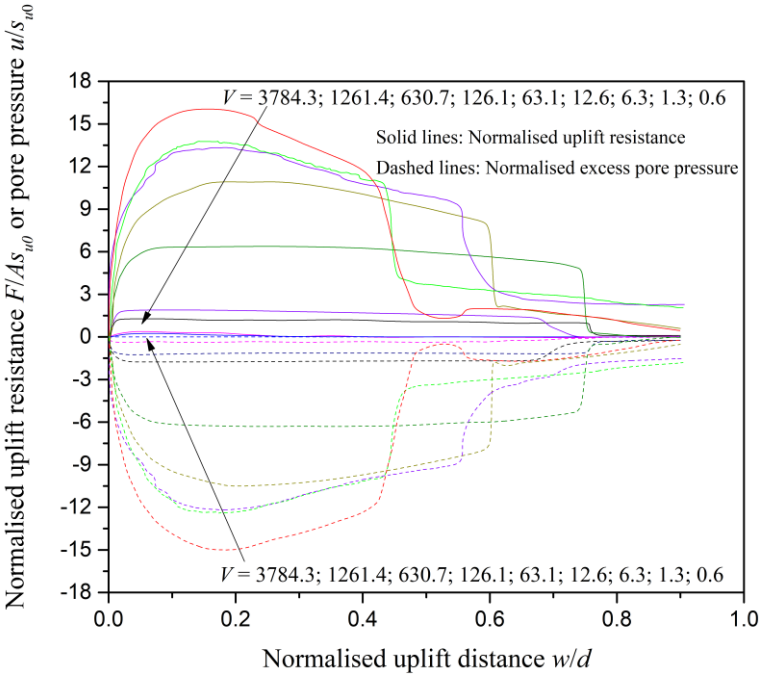

Fig. 2 Results of full model centrifuge tests

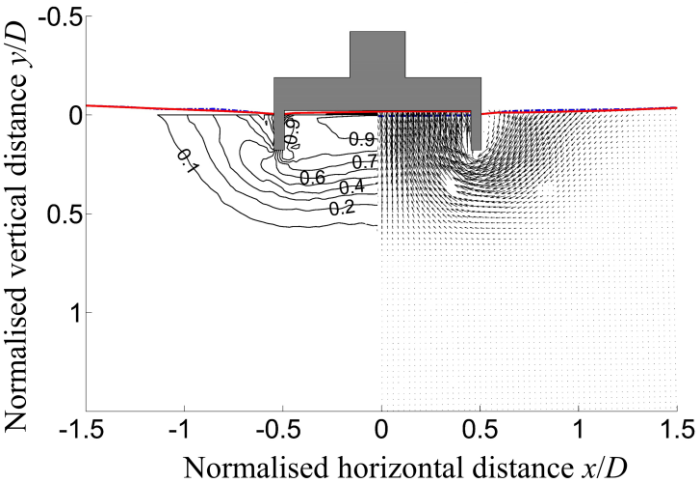

(a) V = 1261.4

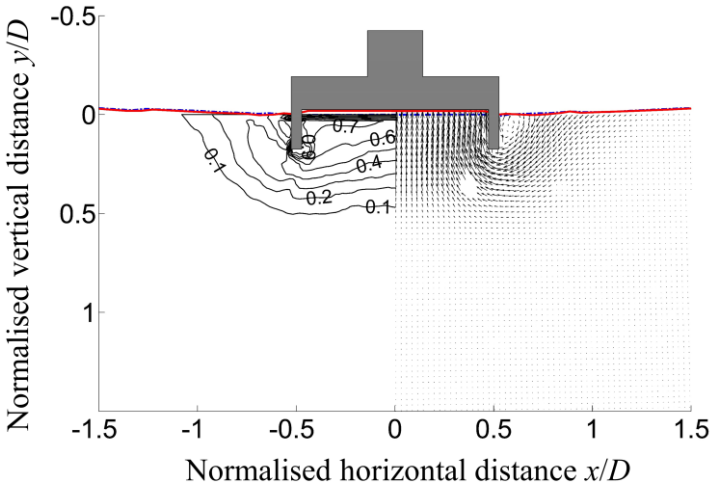

(b) V = 63.1

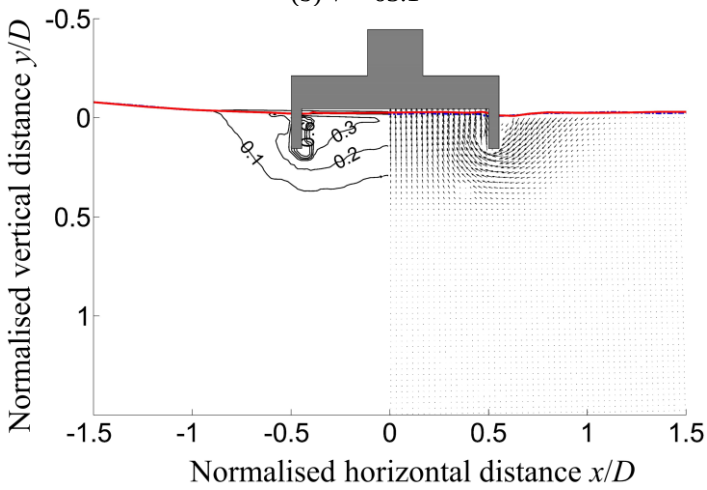

(c) V = 1.3

Fig. 3 Normalised soil displacement contours and failure mechanisms at peak uplift resistance

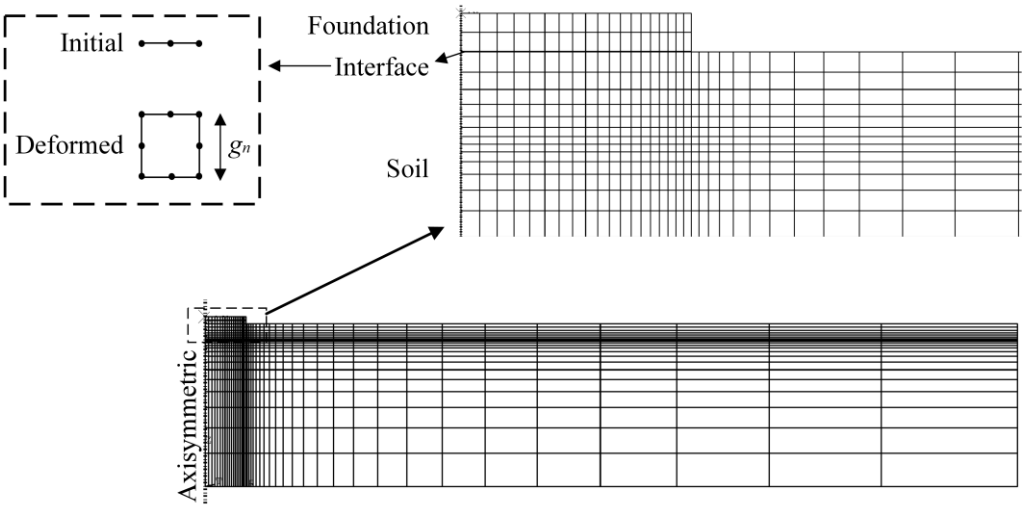

Fig. 4 FE model setup and mesh

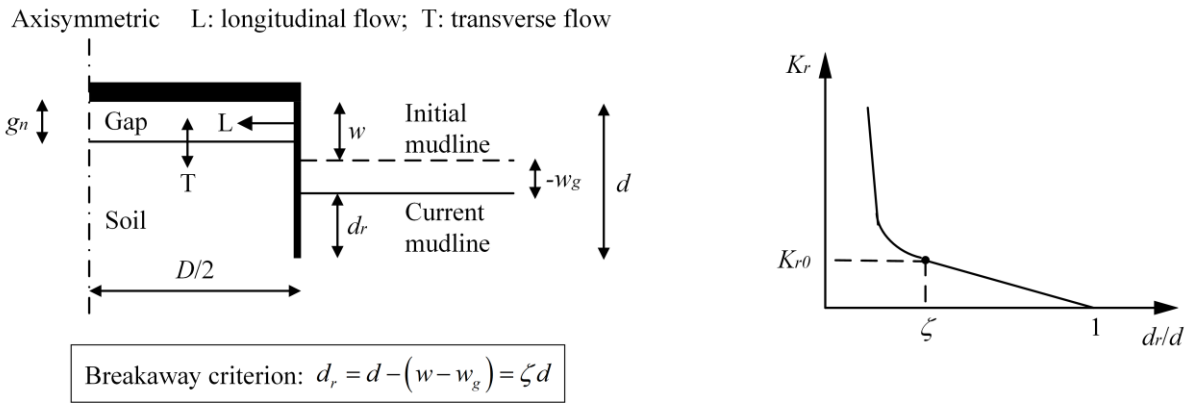

Fig. 5 Schematic illustration of the proposed breakaway criterion

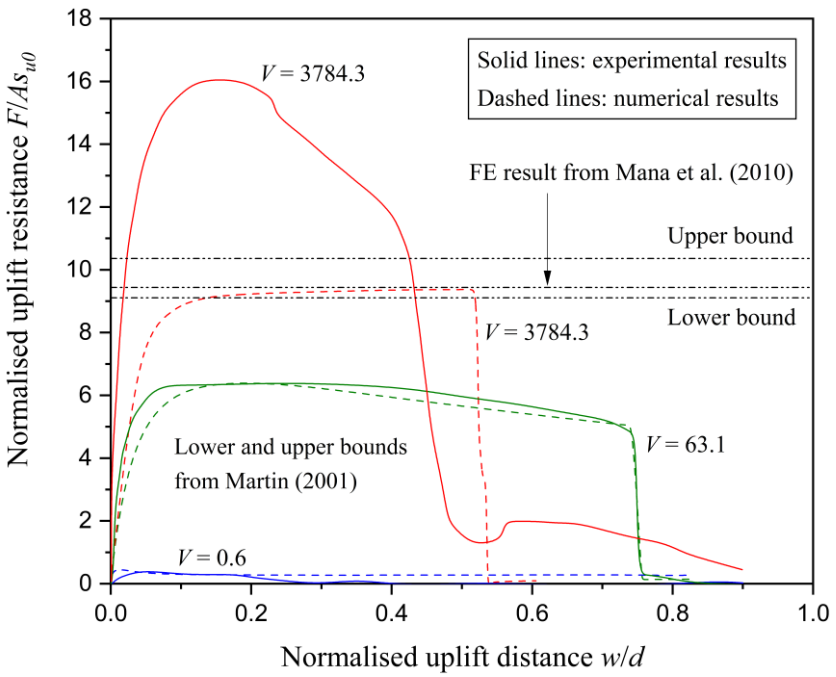

Fig. 6 Comparison between numerical and experimental results

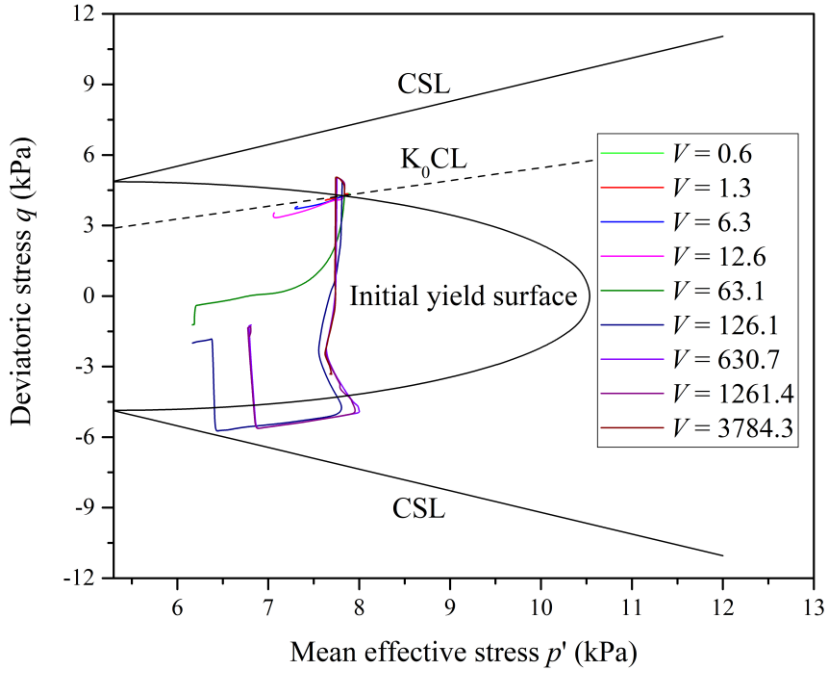

Fig. 7 Stress paths for soil 0.03*D* below the foundation centre at varying velocities

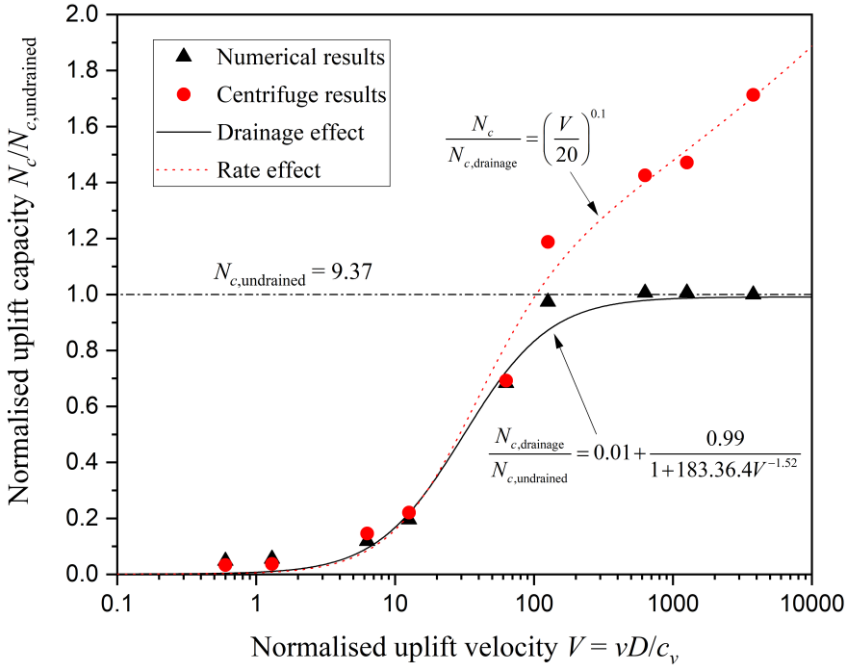

Fig. 8 Numerical and experimental backbone curves

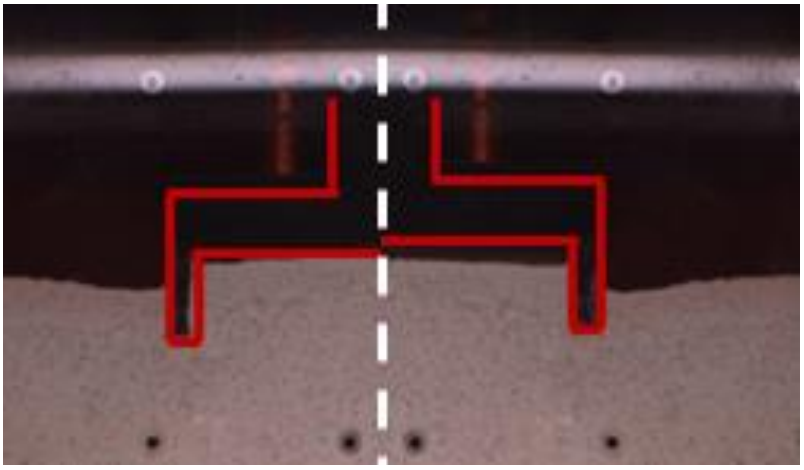

Fig. 9 PIV results before and after breakaway at v = 1 mm/s

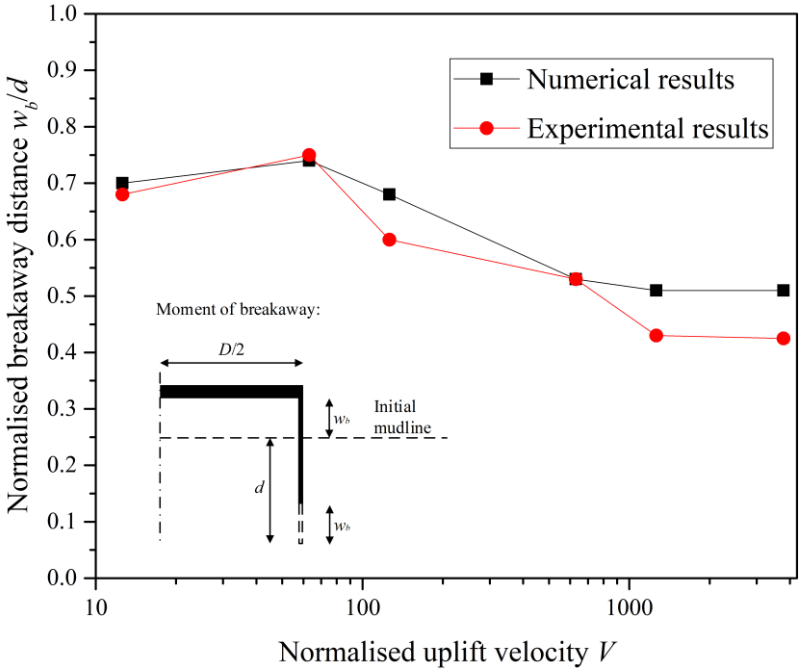

Fig. 10 Comparison of numerical and experimental breakaway distance

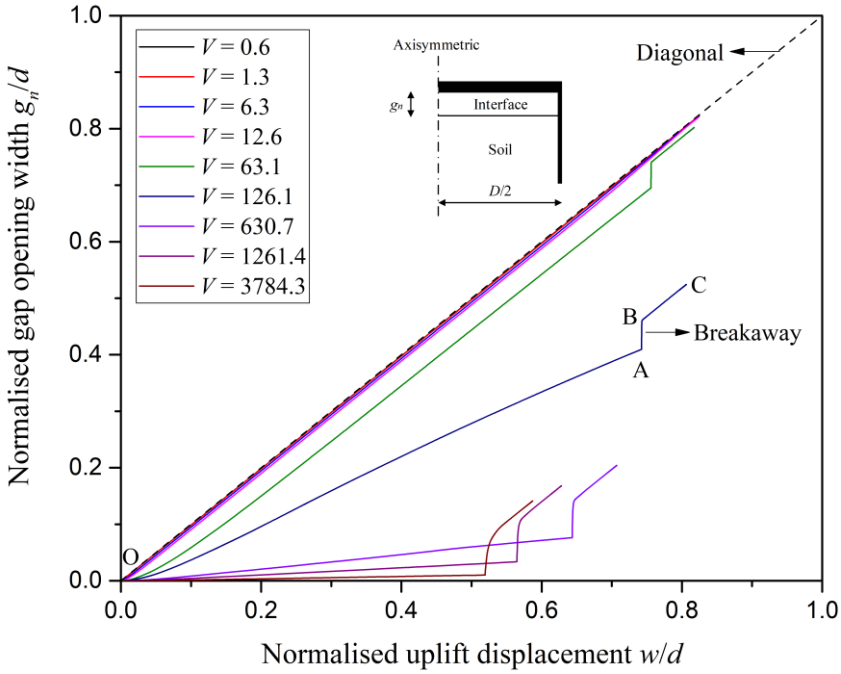

Fig. 11 Evolution of foundation-soil separation distance against uplift distance